MICROWAVE-DETECTED PHOTOCONDUCTANCE DECAY

Paul A. Basore and Barry R. Hansen

Sandia National Laboratories

SAND--89-2464C

DE90 011505

ABSTRACT

Microwave-detected photoconductance decay (μW-PCD) provides a contactless measurement of the recombination lifetime of free carriers in semiconductors following a pulse of optical excitation. Several complications in interpreting the results obtained by this method have prevented its widespread acceptance. In this paper, detailed models are proposed and verified experimentally using a commercially-available apparatus. The model adequately predicts the behavior of the microwave reflectance as a function of wafer conductivity and system configuration. A new light-biased variation of the technique is described which makes it possible to characterize lifetime as a function of excess carrier density. This capability makes it possible to measure the emitter saturation current density for diffusions in high-resistivity wafers, a valuable process control tool.

INTRODUCTION

The measurement of excess carrier recombination lifetime by photoconductance decay takes several forms, differentiated primarily by the method used to detect the change in carrier concentration. Ohmic contacts, photoluminescence, radio-frequency inductive coupling, and microwave reflection have all been applied. Each technique has its particular advantages. Our recent work has dealt with detection by microwave reflection using a commercially-available apparatus (Wafer-τ by Leo Giken). Our goal was to implement contactless in-line process control for silicon wafers in Sandia's Photovoltaic Device Fabrication Laboratory (PDFL), thereby making this measurement technique more accessible to the PV community.

Microwave reflection has several advantages for our application. The high frequency of microwaves combined with a high-speed laser diode for optical excitation permits the accurate measurement of samples with lifetimes ranging from 100 ns to 10 ms without requiring any mechanical reconfiguration or tuning. By outfitting our system with computer control and custom software, each lifetime measurement can be performed in less than 10 s, and maps of lifetime versus position can be obtained with 5-mm spatial resolution.

Previous studies of μW-PCD have confirmed the validity of the method [1], but several aspects of the technique have prevented it from achieving widespread acceptance. Phase-sensitive microwave interference effects and lateral nonuniformities in the optical excitation often yield confusing results, including the observation that the detected microwave reflectance signal changes polarity between low- and high-resistivity wafers [2]. For resistivities near the transition, the result is a markedly non-exponential decay.

This paper examines the μW-PCD apparatus in detail. Models of the microwave and detection circuits are proposed which adequately predict the behavior of the measured microwave reflectance as a function of wafer conductivity and system configuration. This study led us to make several modifications to the apparatus, including development of a new light-biased variation of the technique which makes it possible to measure carrier lifetime as a function of photogenerated carrier density. This capability allows us to measure the emitter saturation current density for diffusions into high-resistivity wafers. With these modifications, we have succeeded in making μW-PCD a reliable, general-purpose process control tool for the PDFL.

THE MICROWAVE CIRCUIT

The microwave components in μW-PCD typically consist of a microwave source, a waveguide, and a circulator for separating the reflected component. As depicted in Fig. 1, the end of the waveguide directs the microwaves through a glass plate onto the bottom of the wafer. In our apparatus, there is also a reflecting metal plate positioned above the wafer, with the distance between the wafer and this plate being adjustable.

This work supported by the Photovoltaic Energy Technology Division, U.S. Department of Energy under contract DE-AC04-76DP00789.

Presented at the 21st IEEE Photovoltaic Specialists Conference, May 1990.

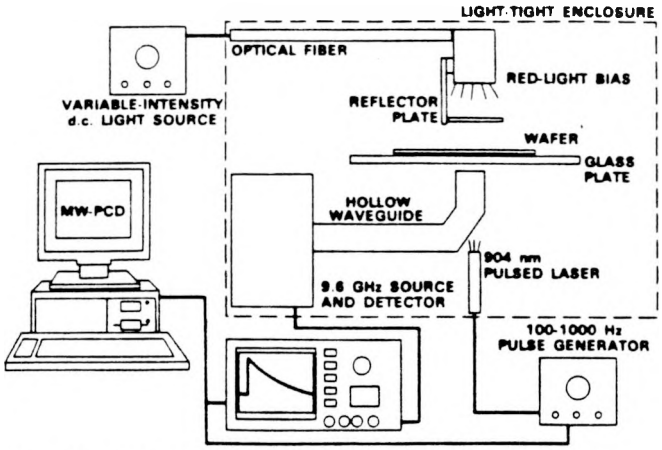

Fig. 1. The PDFL μW-PCD apparatus, based on a commercially-available system, but including several enhancements discussed in this paper.

Beyond the end of the waveguide, the microwaves are essentially planar and normally incident on the dielectric plate and wafer. The interaction of the microwaves thus follows simple one-dimensional wave theory for lossy dielectrics, with the exceptions that one must account for the energy lost by diffraction from the metal plate when it is separated significantly from the wafer, and account for a fixed reflectance due to the abrupt termination of the waveguide. Fig. 2 shows the calculated reflectance as a function of the metal plate separation from the dielectric plate in the absence of a wafer. In performing these calculations, the reflection from the waveguide termination was taken as having an amplitude of 25% of the incident beam and a phase angle with respect to the incident beam of 180°. Diffraction from the reflector plate was included by reducing the effective reflectance at the plate by an exponential function of the air-gap distance, using a spatial decay length of 5 cm. The resulting agreement with the measured values is good, and confirms that the 9.6-GHz signal has the expected wavelength in air of 31 mm. An interesting observation is that a glass plate thickness of 4 mm, rather than the 1 mm in our apparatus, would act as an effective microwave antireflection layer to better couple the microwave energy into the silicon wafer.

Using this model of the microwave circuit, Fig. 3 shows the calculated net reflectance when 500-μm-thick silicon wafers of various sheet conductance are inserted in the beam. Note that the position of the reflector plate has less effect when the wafer conductance is high, because relatively little microwave energy penetrates through the wafer to reach the reflector plate. This does not mean, however, that the microwaves are absorbed within the wafer or are nonuniformly distributed within the wafer. Even at the upper limit of conductance shown in Fig. 3, 50 mS, the microwave skin depth is still larger than the assumed 500 μm wafer thickness. Repeating this calculation for other values of wafer thickness reveals that the microwave reflectance depends primarily on the sheet conductance (sheet resistance) and not on the

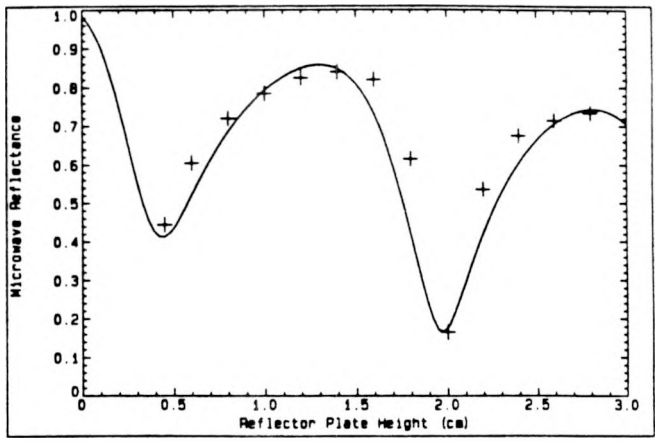

Fig. 2. The calculated microwave reflectance (solid line) compared to experimental values (crosses) as a function of the distance of the reflector plate from the glass sheet, in the absence of a wafer.

wafer conductivity (resistivity), as long as the skin depth remains larger than the wafer thickness. It is for this reason that we refer to this technique as "photoconductance decay," rather than the more commonly cited "photoconductivity decay."

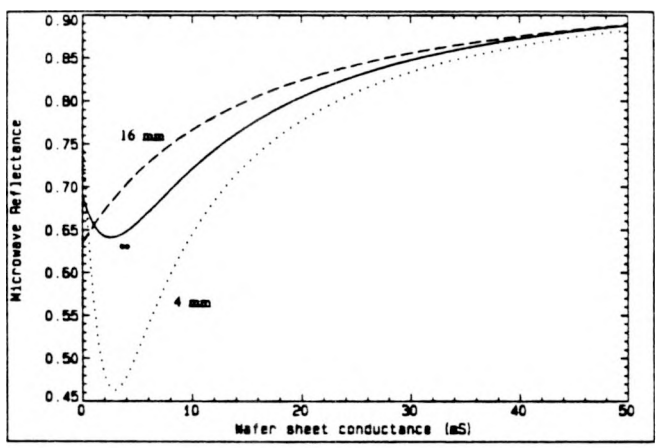

Fig. 3. The calculated microwave reflectance as a function of the sheet conductance of a 500-μm-thick silicon wafer for reflector-plate positions corresponding to three different air-gap spacings.

THE DETECTOR CIRCUIT

The 904-nm laser diode injects about $2 \cdot 10^{12}$ photons per pulse at its highest power setting, with a pulse duration of less than 100 ns. For a typical beam diameter of 2 mm and wafer thickness of 500 μm, this generates an excess carrier density of about $1 \cdot 10^{15}$ cm^{-3}. These excess carriers increase the wafer conductance, averaged over the 2.5-cm^2 microwave beam area, by about 0.2 mS, or less than 0.5% of the abscissa in Fig. 3. The change in net microwave reflectance due to laser photogeneration is therefore only a small fraction of the steady-state reflectance, and the sign of the reflectance change due to laser excitation may be either positive or negative, depending on the wafer

conductance and the reflector plate position.

Although Fig. 3 suggests that there is a reflector position that avoids the critical transition between decreasing and increasing reflectance versus wafer conductance, this position represents an interference null that is difficult to locate reliably. A positioning error of 1 mm or a change in the wafer thickness of 10% is enough to upset the balance and restore the critical transition. Thus, when measuring wafers with a conductance between 2 mS (500 Ω/□) and 5 mS (200 Ω/□), it is generally necessary to adjust the position of the reflector plate to avoid the critical transition point. Fortunately, relatively few wafers of photovoltaic interest fall within this range.

Fig. 3 also illustrates another important limitation of the μW-PCD method. Note that the reflectance becomes less sensitive to laser excitation as the wafer conductance increases. We have found that this limits the usefulness of the μW-PCD technique to wafers with a sheet conductance of less than 100 mS (sheet resistance greater than 10 Ω/□). This generally precludes applying this method to metallized wafers.

The reflected microwave signal is detected by rectification, creating a voltage across a load resistor proportional to the amplitude of the reflected microwave beam. The result is a d.c. voltage, the value of which depends on the wafer conductance and reflector plate position, onto which is imposed a small variation resulting from laser excitation. This variation in voltage is linearly proportional to the change in wafer conductance, which in turn is proportional to the photogenerated carrier density averaged over the thickness of the wafer. Note that this spatial averaging of the carrier density makes this technique less sensitive to carrier-diffusion effects than electrically-contacted transient decay techniques, which are sensitive only to the carrier density at the pn junction.

In order to amplify separately the small signal due to photogeneration, a high-pass filter (a.c. coupling) is used to block the d.c. voltage component. In the Leo apparatus, a second high-pass filter is located at the input to the A/D converter. The time constant of these filters (≈ 10 ms) can create significant errors in measuring long lifetimes.

The signal digitization technique used in the Leo apparatus is a sampling method that pulses the laser repeatedly, measuring one point on the decay curve for each pulse (starting after the fourth pulse). If signal averaging is requested, then the process is repeated for the specified number of replications. Thus, a 128-point digitization of the decay curve with 100 decay curves averaged requires 100•(128+4) = 13,200 pulses of the laser. At the maximum pulse repetition rate of 1 kHz, this takes 13.2 seconds to complete. On this extended time scale, the signal at the output of the high-pass filter relaxes to a periodic waveform for which the time-average of the voltage is zero, and all information regarding the original background reflectance voltage is lost. This introduces quite a complication. Knowledge of the background voltage is essential to determination of the decay lifetime, which is the ratio of the deviation of the voltage from its background value to the slope of the voltage at each point on the decay curve. The method used in the Leo apparatus is to identify the voltage at the end of the decay following the first laser pulse (for each decay curve averaged) as the background voltage for that decay curve. This works well when the carrier lifetime is somewhat shorter than both the laser repetition period and the high-pass-filter time constant.

Fig. 4 shows what happens when the carrier lifetime approaches the laser repetition period. Because the carriers have not all recombined when the next laser pulse arrives, the carrier concentration builds up with each additional laser pulse. This competes with the relaxation of the waveform due to the high-pass filter, yielding the results shown in the figure. It is apparent in this figure that the voltage at the end of the first transient decay is a very poor estimate of the background voltage, and large errors in calculating the lifetime result.

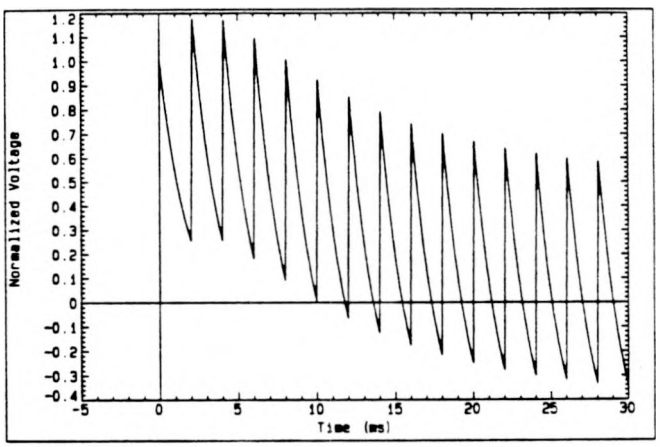

Fig. 4. Illustration that substantial waveform shifts can be introduced when the carrier lifetime approaches the pulse repetition period.

It is possible to correct the measured data to account for the combined effects of the high-pass filter and pulse repetition rate when the impact of these effects is not too severe. Fig. 5 shows the calculated apparent lifetime as a function of the actual carrier decay lifetime. The number of decay curves averaged affects the plot because only the first of the averaged curves is subject to the start-up transient shown in Fig. 4. Fig. 5 can be used in reverse to infer the true lifetime from the measured lifetime. The measured data shown in Fig. 5 verifies the predicted dependence on pulse repetition rate for a particular sample.

MODIFICATIONS TO THE APPARATUS

The previous discussion was based on the commercially-available Leo Giken Wafer-τ System 1303, composed of separate units identified as models LTA-130A, WA-1, and WA-2. In this section we will present a series of modifications which we

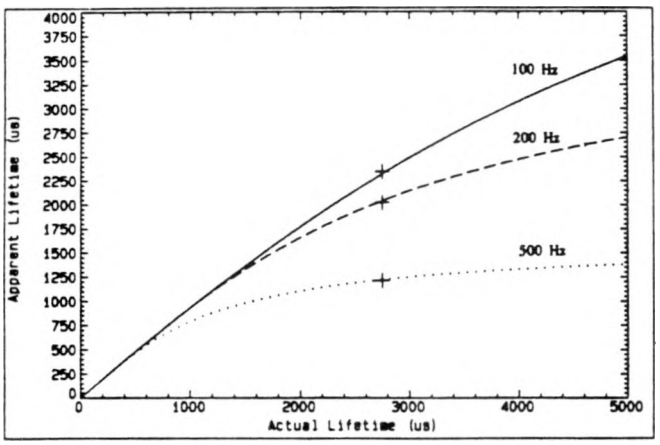

Fig. 5. Relationship between measured and actual decay lifetime for a high-pass time constant of 15 ms with 10 decay curves averaged. The crosses indicate the measured lifetime of a particular sample at the three pulse rates shown.

have made to this apparatus which substantially enhance its accuracy for long-lifetime materials, and its overall utility as an in-process lifetime monitor. These modifications are reflected in the diagram of Fig. 1.

The first and simplest modification was to remove the high-pass filter in the A/D converter by shorting across the input capacitor. As long as the d.c. offset voltage in the preceding signal amplifier is adequately nulled, this introduces no difficulties and increases the net effective high-pass time constant from less than 10 ms to about 15 ms, the value used in the calculation of Fig. 5. The time constant was measured using a digital storage oscilloscope to observe the turn-off transient following a series of laser pulses.

Another simple, yet important, modification made to the apparatus was to cover the inner surface of the rubber hand-holds on the lid of the light-tight enclosure with metal tape. These hand-holds were found to introduce a significant amount of noise by allowing both 60-Hz interference and room light to penetrate the measurement enclosure.

The computer program supplied with the Wafer-τ is rather slow and cumbersome, being written in interpretive BASIC. We have written a substantially more effective program in compiled Pascal, MW-PCD, which implements a mouse-driven menu interface for setting parameters and which takes full advantage of high-resolution graphics on an IBM PS/2 personal computer to display results. The program can automatically correct for the high-pass time constant and pulse-repetition frequency effects that were illustrated in Fig. 5. This computer program is currently available at no charge from the authors.

MW-PCD includes the ability to drive the x-y stage in the Wafer-τ to collect lifetime data from multiple points and compute statistics based on this data. Fig. 6 shows a map of carrier lifetime as a function of position for a 100-mm diameter wafer. The map was constructed by smoothing the data collected from 85 separate locations. This high-resistivity wafer, grown by the magnetically-stabilized Czochralski (MCZ) technique had received a phosphorous diffusion on both sides and a surface-passivating dry oxidation. This map shows that the lifetime, while variable, is excellent across the entire wafer surface.

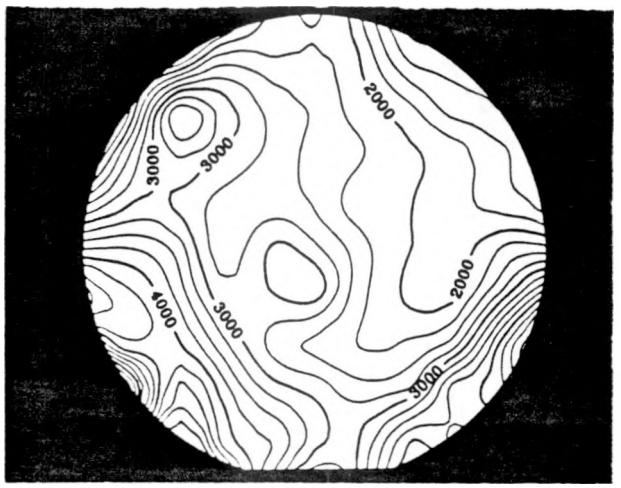

Fig. 6. PCD lifetime, in μs, for a diffused high-resistivity MCZ wafer processed in our laboratory.

A particularly valuable feature of the MW-PCD program is an automatic setup routine that collects just enough data from the Wafer-τ to determine appropriate settings for the input sensitivity, sampling interval, number of points, number of averages, and pulse repetition rate. This makes the system usable on a routine basis in the PDFL to collect data from a wide variety of materials with lifetimes ranging from less than 1 μs to over 1 ms, without requiring a detailed understanding by the operator of the limitations of the apparatus.

The preceding improvements, culminating in version 2.2 of MW-PCD, served our purpose for several months. But we eventually became impatient with the speed with which the data was collected. The sampling approach used in the Leo apparatus typically leads to data collection times exceeding 10 seconds per point. When sampling multiple points per wafer this can become a tedious process. Digital storage oscilloscopes are now available that can digitize the entire decay waveform from a single laser pulse. When averaging the same number of waveforms, this approach can reduce the direct data collection time by two orders of magnitude. After accounting for overhead time associated with moving the x-y stage and communicating the data to the computer, it is possible to increase significantly the number of waveforms averaged to obtain better precision, while still reducing substantially the time required to complete each measurement. We have implemented this strategy using a Hewlett-Packard model 54501A digital storage oscilloscope which communicates with the computer via GPIB. With this enhancement, the Leo signal-processing unit (WA-2) is used only to set

the laser repetition frequency. As illustrated in Fig. 1, this job could be adequately performed by any computer-controlled pulse generator.

By using an independent oscilloscope for data collection, it is possible to turn on the laser and let the waveform settle to its periodic steady state before collecting any data. The high-pass time constant can therefore be increased without introducing errors due to the turn-on transient illustrated in Fig. 4. We have increased this time constant in our apparatus to 150 ms by adding a parallel capacitor to the coupling circuit.

LIGHT-BIASED LIFETIME MEASUREMENTS

One final modification that we have implemented in our apparatus is the addition of d.c. light bias. Measurement of the decay lifetime under bias illumination often provides a better indicator of potential photovoltaic performance than measurements made in the dark. A stable, feedback-controlled lamp is coupled via optical fiber into the measurement enclosure. The upper laser that was supplied with the apparatus and the reflector plate were removed to make room for the optical fiber. A translucent plastic screen is used to diffuse the light as it exits the fiber so that it illuminates the wafer under test with a beam diameter of about 75 mm. The maximum bias-light intensity corresponds to about one-sixth sun.

Our lamp source (Newport model 770) has an intensity that is switch-selectable in 10% increments. This provides the opportunity for characterizing PCD lifetime as a function of excess carrier density. In order to quantify the observed variation in lifetime, it is necessary to relate the excess carrier concentration in the wafer to the lamp intensity. Due to the nonlinear effects of phase-sensitive interference, it is not feasible to infer the excess carrier density directly from the microwave reflectance signal. Instead, a solar cell with near-unity short-circuit carrier collection efficiency (Stanford S22-1-1) is used to determine the photogeneration rate in the cell per unit area, as a function of the control setting on the bias-light source. The photogeneration rate per unit area in the wafer under test should be similar, and can be estimated to within about 5% accuracy by taking into account differences in surface texture, antireflection coatings, and thickness. To minimize uncertainty in this estimate, it is best if the bias light spectrum is dominated by wavelengths for which the absorption coefficient in silicon is such that most of the light is absorbed beyond the near-surface region (minimizing emitter quantum efficiency effects) but still on its first pass through the thickness of the wafer (minimizing light-trapping effects). We use a piece of red plastic film to filter out most of the rapidly-absorbed light without excessively reducing the total photogeneration rate.

For planar oxidized wafers we have used PC-1D/2 [3] to construct a plot of wafer photogeneration responsivity as a function of oxide and wafer thickness. This plot is shown in Fig. 7. The ratio of the wafer responsivity from this plot to the responsivity calculated for the reference solar cell (0.397 A/W), times the photogeneration rate measured by the solar cell (up to $4 \cdot 10^{16}$ cm^{-2}/s), gives the estimated photogeneration rate for the wafer under test.

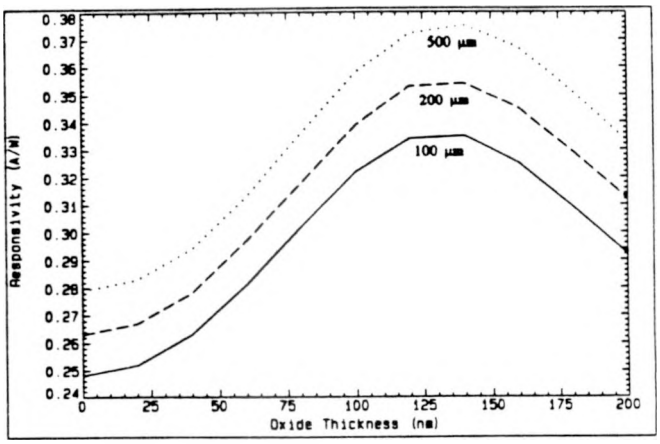

Fig. 7. Plot used to infer the photogeneration rate due to red-light bias in planar wafers.

It was found necessary to defocus the laser in order to reduce the carrier density due to the laser to a small fraction of the carriers generated by the bias light. By removing the lens from in front of the laser, the beam size was increased from 2 mm to more than 5 mm, thereby reducing the effective laser photogeneration rate per unit area to less than 10% of that due to the bias illumination. The total number of carriers generated per pulse remains the same, however, so that the signal strength is not diminished.

Because there are no external outlets for excess carriers, the total photogeneration rate per unit area, Γ, must be matched by recombination within the wafer. For a wafer of thickness w and diffusivity D, with recombination dominated by processes proportional to the bulk excess carrier concentration, and minority-carrier diffusion transit time ($w^2/\pi^2 D$) short compared to the observed lifetime, τ, the resulting excess carrier concentration is approximately uniform, and given by

$$n = \Gamma\tau/w. \qquad (1)$$

For low-resistivity wafers (those which remain in low-level injection under bias illumination), equation (1) is still applicable when a surface diffusion of either n- or p-type polarity is added. For diffused high-resistivity wafers the situation is somewhat more complex. Assume that recombination at the two diffused surfaces can be characterized by an average emitter saturation current density per side, J_{oe}, and that at the carrier concentrations utilized, Auger recombination is negligible. The total recombination rate per unit area, R, for a given background doping density, N, and uniform excess carrier density in the bulk, n, is given by

$$R = (w/\tau_b)\cdot n + (2J_{oe}/qn_i^2)\cdot n\cdot(N+n), \qquad (2)$$

where τ_b is the carrier lifetime in the bulk, and n_i is the intrinsic carrier concentration. The PCD lifetime, τ, for small perturbations of the excess carrier density (n') with respect to the background carrier density produced by the light bias, is

$$1/\tau = (1/\tau_b + 2J_{oe}N/qwn_i^2) + (4J_{oe}/qwn_i^2)\cdot n'. \quad (3)$$

Equating the total recombination rate to the photogeneration rate, a linear relationship can be obtained between the measured lifetime and the photogeneration rate due to light bias,

$$1/\tau^2 = (1/\tau_b + 2J_{oe}N/qwn_i^2)^2 + (8J_{oe}/qn_i^2w^2)\cdot\Gamma. \quad (4)$$

By plotting $1/\tau^2$ versus Γ, the slope of the resulting line can be used to calculate J_{oe}. Knowledge of the doping density then permits the intercept of the line to be used to estimate the bulk lifetime, although we have found that this intercept is quite sensitive to both random measurement errors and the small increase in carrier density resulting from laser excitation.

Fig. 8 illustrates data for five different light-bias intensities for the center point of the wafer illustrated in Fig. 6, and the resulting fit for J_{oe}. The lifetime data collected using this technique is nearly independent of temperature, because J_{oe} has essentially the same temperature dependence as n_i^2. J_{oe} values are usually quoted at 300 K, which simply requires that the desired 300 K value of n_i be used in equation (4), even though the data may have been collected at room temperature.

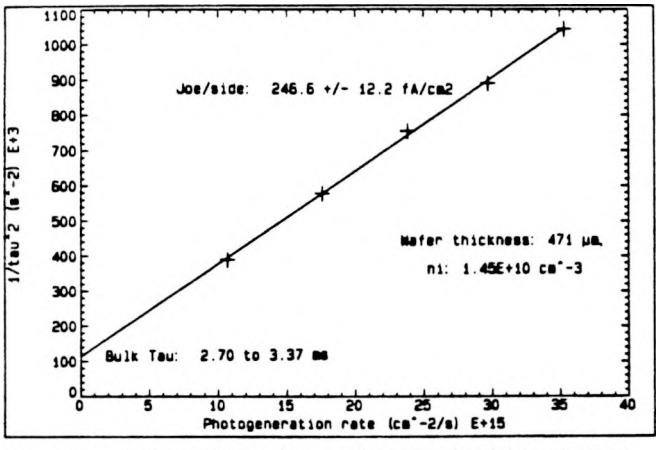

Fig. 8. Extraction of J_{oe} from light-biased data.

It is therefore possible by this technique to accurately measure the emitter saturation current density using a diffused high-resistivity wafer. Because the emitter saturation current density is essentially unaffected by the resistivity of the bulk, the value of J_{oe} obtained from a high-resistivity test wafer should also apply when the same diffusion process is applied to low-resistivity wafers.

To test the validity of this method of measuring J_{oe}, four wafer samples with different emitter diffusions were measured at Stanford University using the inductively-coupled PCD technique [4]. Table 1 lists the results obtained by each method, with confidence limits as indicated. The agreement is good over a wide range of emitter diffusions.

Table 1
Emitter Saturation Current Density Comparison
Sandia: µW-PCD, Stanford: Inductively-coupled PCD

Wafer ID	Thickness µm	J_{oe}/side at 300 K (fA/cm^2) Stanford	Sandia
B4F-3-Ub	273	34 ± 1	40 ± 2
A4F-3-Ub	273	45 ± 2	54 ± 2
A1-FL-Ud	210	186 ± 6	194 ± 17
A3-OL-Ud	211	870 ± 80	744 ± 260

CONCLUSIONS

We have studied in detail the characteristics of microwave-detected photoconductance decay and have determined that, with proper interpretation and some equipment modifications, this technique provides a simple, fast, and reliable measurement of the recombination lifetime in wafers having a sheet resistance above 10 Ω/□, with special care required in the range 200-500 Ω/□. This lifetime represents recombination throughout the wafer. Bulk, surface, or diffused-region recombination can be emphasized by proper selection of the test wafer's resistivity and surface treatment. We have successfully implemented this technique for routine in-line process control in the PDFL for both oxidation and diffusion processes.

ACKNOWLEDGMENTS

The authors wish to thank Tsuyoshi Uematsu of Hitachi, Ltd., who breached the language barrier we had faced with the Japanese manufacturer of our µW-PCD apparatus, thereby giving us the confidence to undertake this development effort. Also, we appreciate the comparison measurements of J_{oe} performed by Richard King at Stanford University.

REFERENCES

[1] J.M. Borrego, R.J. Gutmann, N. Jensen, and O. Paz, "Non-destructive Lifetime Measurement in Silicon Wafers by Microwave Reflection," Solid-State Electronics, 30 (2), 1987, pp. 195-203.

[2] M. Kunst and G. Beck, "The Study of Charge Carrier Kinetics in Semiconductors by Microwave Conductivity Measurements," J. Applied Physics 60 (10), Nov 1986, pp. 3558-3566.

[3] P.A. Basore, "Numerical Modeling of Textured Silicon Solar Cells Using PC-1D," IEEE Trans. on Electron Devices, ED-37 (2), Feb 1990, pp. 337-343.

[4] D.E. Kane and R.M. Swanson, "Measurement of the Emitter Saturation Current by a Contactless Photoconductivity Decay Method," Conf. Rec. of the 18th IEEE Photovoltaic Specialists Conf., Las Vegas, Oct 1985, pp. 578-583.

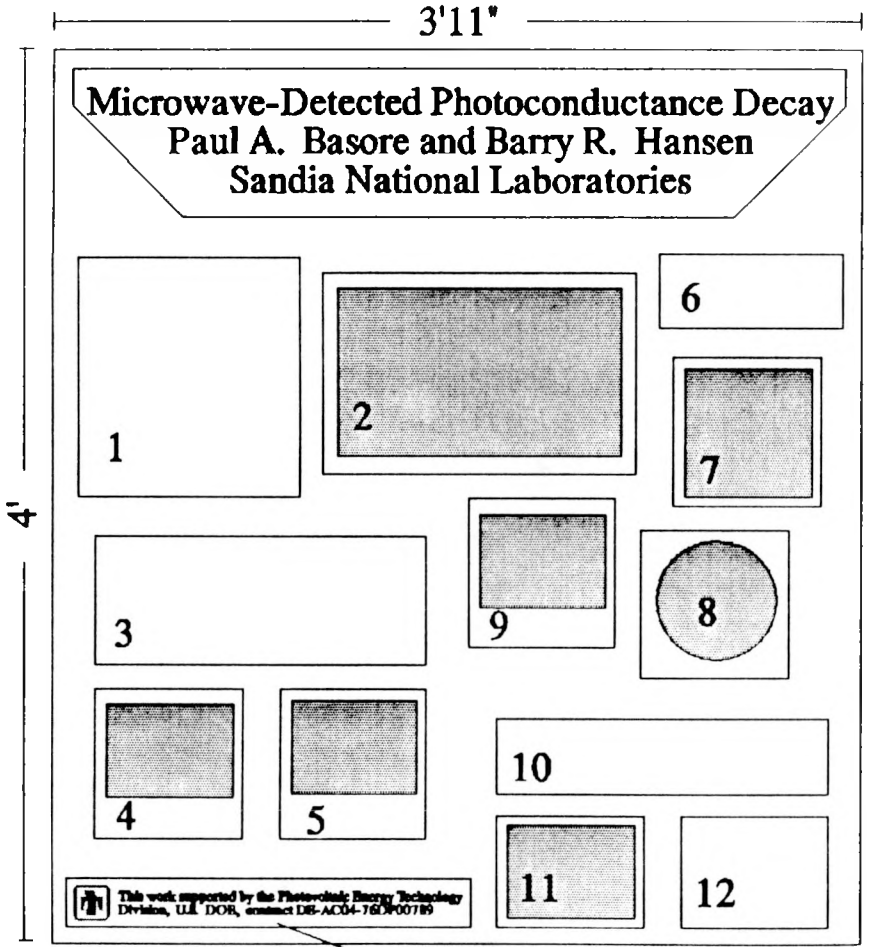

1. Abstract text, to be typeset on 12"x13" mat.
2. Schematic diagram of apparatus, to be generated by Genigraphics for mounting on a 17"x11" mat.
3. Explanatory text for mounting on a 18"x7" mat.
4. B&W graph of Reflectance vs. Plate Location, 8" square mat. Caption: Calculated microwave reflectance (solid line) compared to experimental values (crosses), in the absence of a wafer.
5. B&W graph of Reflectance vs. Wafer Conductance for mounting on a 8" square mat. Caption: Calculated microwave reflectance versus wafer sheet conductance for several reflector plate positions.
6. Explanatory text for mounting on a 10"x4" mat.
7. 7" square print of computer from 35mm color negative, mounted on a 8" square mat.
8. B&W wafer diagram, mounted with the flat edge down, 8" square mat. Caption: Lifetime (μs)
9. B&W graph of Voltage vs. Time, 8" square mat. Caption: Typical transient decay of detected microwave voltage following a laser pulse.
10. Explanatory text for mounting on a 18"x4" mat.
11. B&W graph of 1/tau^2 vs. Photogeneration Rate, for mounting on a 8"x6" mat. No caption needed.
12. Table comparing Sandia & Stanford measurements, to be typset and colorized on a 8"x6" mat.

Contact: Paul A. Basore, 6224, 6-4516
Date required, with all corrections: 5/17/90

This work supported by the Photovoltaic Energy Technology Division, U.S. DOE, contract DE-AC04-76DP00789

BLOCK #1 (12"x13" mat)

Microwave-Detected Photoconductance Decay
(μW-PCD)

- Provides a contactless, in-process technique for measuring the recombination lifetime in a semiconductor wafer following an optical pulse
- Can measure lifetimes from 100 ns to 10 ms in less than 10 s, with no mechanical adjustments
- Can map lifetime with 5-mm spatial resolution
- Is equally sensitive to recombination throughout the wafer thickness, including both surfaces
- Has not yet been widely accepted because it often yields confusing results due to microwave interference effects and lateral nonuniformities

The study of μW-PCD reported here explains these effects in detail for a specific apparatus, and extends the technique to include the measurement of emitter saturation current density.

BLOCK #3 (18"x7" mat)

Microwaves are passed through a waveguide, reflect off the wafer, and are detected upon their return. The laser creates additional free carriers in the wafer that increase its microwave reflectance until they recombine. The microwaves reflected from the wafer interfere with reflections from the glass plate and the reflector plate located above the wafer.

The left figure below demonstrates that the complex net microwave reflectance of this system can be adequately calculated using a planar-interference model. The right figure uses this model to calculate the effect of wafer conductance on the net reflectance. Note that for low initial sheet conductance (high-resistivity wafers), the addition of laser-injected carriers can actually decrease, rather than increase, the net microwave reflectance.

BLOCK #6 (10"x4" mat)

A computer program for IBM-PCs and compatibles has been written to automate the setup and collection of μW-PCD lifetime data. The computer drives an x-y stage to measure lifetime uniformity.

BLOCK #10 (18"x4" mat)

By removing the reflector plate and inserting a red-light bias source, lifetime measurements as a function of background carrier density can be obtained using emitter-diffused high-resistivity wafers. From this, the emitter saturation current density can be determined. The results compare well with those obtained using a different technique at Stanford University.

BLOCK #12 (8"x6" mat)

Emitter Saturation Current Density
fA/cm^2 per side
using $n_i = 1.45 \cdot 10^{10}\ cm^{-3}$

Sample	Sandia	Stanford
B4F-3-Ub	40 ± 2	31 ± 4
A4F-3-Ub	54 ± 2	45 ± 5
A1-FL-Ud	194 ± 17	194 ± 15
A3-OL-Ud	744 ± 260	780 ± 450